

Multipole relaxation in 5^2P potassium atoms by collisions with He, Ne, and Ar

R. W. Berends, W. Kedzierski, and L. Krause

Department of Physics, University of Windsor, Windsor, Ontario, Canada N9B 3P4

(Received 18 May 1987)

Potassium vapor, contained together with a buffer gas in a fluorescence cell located in a 7-T magnetic field, was irradiated with light from a pulsed dye laser producing selective excitation of the $5^2P_{1/2, -1/2}$ or the $5^2P_{3/2, -3/2}$ Zeeman substate. Collisions of the excited and polarized atoms and the resulting Zeeman mixing produced a population of the whole Zeeman manifold and resulted in the emission of a fluorescent Zeeman spectrum which was resolved with a Fabry-Perot interferometer and registered with a photomultiplier and multichannel scaler. Measurements of the relative intensities of the fluorescence components yielded the absolute (thermally averaged) multipole-relaxation cross sections and cross sections for Zeeman mixing by collisions with He, Ne, and Ar atoms.

I. INTRODUCTION

The depolarization of excited alkali-metal atoms, induced in collisions with various atoms and molecules, has been the subject of several experimental and theoretical studies.¹ Cross sections for m_j mixing and multipole relaxation in 3^2P sodium atoms by collisions with ground-state sodium and noble-gas atoms were determined by Gay and Schneider.^{2,3} Similar cross sections for 4^2P potassium atoms were reported by Boggy and Franz⁴ and by Skalinski and Krause,⁵ while Berends *et al.*⁶ measured cross sections for depolarization of 4^2P potassium atoms by collisions with N_2 and H_2 . Lewis *et al.*⁷ carried out a calculation of $K(4^2P)$ -Ar depolarization cross sections and the cross sections for depolarization by resonant collisions with K atoms were calculated by Carrington *et al.*⁸ Although most of the experimental and theoretical studies of collisional depolarization of excited atoms have dealt with the first resonance states, Spielfiedel *et al.*⁹ have reported an extensive experimental and theoretical treatment of the potassium 5^2P states, dealing mainly with the broadening and shift of the spectral lines, which included a calculation of multipole-relaxation cross sections for collisions with noble-gas atoms.

In this investigation we report the results of an experiment in which we excited selected $5^2P_{J,m}$ Zeeman substates of potassium atoms in a magnetic field of 7 T, and followed the transfer of population among the Zeeman substates, induced by He, Ne, or Ar collisions. The resulting Zeeman spectrum consisting of six fluorescence components was resolved with a Fabry-Perot interferometer and measurements of the relative intensities yielded the various multipole-relaxation cross sections and transfer cross sections. With the fluorescing vapor-gas mixture placed in a relatively strong magnetic field, the electronic and nuclear moments in the potassium atoms were effectively decoupled from each other and the measured cross sections were not affected by the "flywheel effect" of the nucleus.¹⁰

Experimental measurements of cross sections for mul-

tiple relaxation and excitation transfer induced by collisions of excited alkali-metal atoms with ground-state noble gases provide a useful check of theoretical interatomic interaction potentials.¹

II. THEORETICAL

When a potassium atom, excited to a $5^2P_{J,m}$ Zeeman substate, collides with a noble-gas atom, it may be transferred to another m_j substate. Because of the small 5^2P fine-structure splitting, the collisional transfer will span all six Zeeman substates of the 5^2P manifold. The population vector \mathbf{N} describing the population densities of the Zeeman substates must, accordingly, be six dimensional. The time evolution of the population-density vector may be described as follows, using density-matrix formalism in its irreducible tensor representation:^{1,6}

$$d\mathbf{N}/dt = \mathbf{S} - \hat{\Gamma}\mathbf{N} - \hat{\gamma}\mathbf{N}, \quad (1)$$

where \mathbf{S} represents the optical excitation rate of the Zeeman states, $\hat{\Gamma}$ is a matrix describing the spontaneous decay rate of the excited state to the ground state, and $\hat{\gamma}$ is a matrix describing the rate of collisional relaxation between all six Zeeman substates. When the optical excitation takes place by means of laser pulses, Eq. (1) can be integrated¹¹ to yield the following expression for the population of the excited state in terms of the spontaneous decay, collisional transfer, and optical excitation rates:

$$\mathbf{S} - \hat{\Gamma}\bar{\mathbf{N}} - \hat{\gamma}\bar{\mathbf{N}} = 0, \quad (2)$$

where the horizontal bars indicate time-integrated quantities. $\bar{\mathbf{N}}$ may be expressed in terms of multipole densities $n^{(L)}$ which are related to the population densities of the Zeeman substates, $N_{J,m}$.^{5,1} Also, since the system is collisionally isotropic, the components of $\hat{\gamma}$ are rotationally invariant and Eq. (2) may be expressed in terms of the appropriate multipole densities:¹

$$\begin{bmatrix} \Gamma_1 + \gamma_{11}^{(L)} & \gamma_{12}^{(L)} \\ \gamma_{21}^{(L)} & \Gamma_2 + \gamma_{22}^{(L)} \end{bmatrix} \begin{bmatrix} n_1^{(L)} \\ n_2^{(L)} \end{bmatrix} = \begin{bmatrix} s_1^{(L)} \\ s_2^{(L)} \end{bmatrix}. \quad (3)$$

$\gamma_{11}^{(L)}$ and $\gamma_{22}^{(L)}$ are the multipole-decay rates for the $5^2P_{1/2}$ and $5^2P_{3/2}$ states, respectively, $\gamma_{12}^{(0)}$ and $\gamma_{21}^{(0)}$ are the fine-structure-transfer rates corresponding to the ($5^2P_{1/2} \rightarrow 5^2P_{3/2}$) and ($5^2P_{3/2} \rightarrow 5^2P_{1/2}$) transitions, respectively, and $\gamma_{ij}^{(1)}$ and $\gamma_{ij}^{(2)}$ are the fine-structure orientation-transfer rates. All other $\gamma_{ij}^{(L)}$ ($i \neq j$) terms vanish by virtue of the symmetry relations to which $\hat{\gamma}$ is subject.⁶

Various definitions of the fine-structure-transfer rates and orientation-transfer rates may be found in the literature,^{1,4,12} the essential difference among them lies in the normalization factors. We use the following definitions which may be directly derived from Eq. (83) of Baylis:¹

$$\gamma_{12}^{(0)}(\frac{1}{2} \rightarrow \frac{3}{2}) = (1/\sqrt{2}) \sum_m \gamma(\frac{1}{2}, -\frac{1}{2} \rightarrow \frac{3}{2}, m), \quad (4)$$

$$\gamma_{21}^{(0)}(\frac{3}{2} \rightarrow \frac{1}{2}) = \sqrt{2} [\gamma(\frac{3}{2}, -\frac{3}{2} \rightarrow \frac{1}{2}, -\frac{1}{2}) + \gamma(\frac{3}{2}, -\frac{3}{2} \rightarrow \frac{1}{2}, \frac{1}{2})], \quad (5)$$

$$\begin{aligned} \gamma_{12}^{(1)}(\frac{1}{2} \rightarrow \frac{3}{2}) &= (1/\sqrt{10}) [3\gamma(\frac{1}{2}, -\frac{1}{2} \rightarrow \frac{3}{2}, -\frac{3}{2}) \\ &+ \gamma(\frac{1}{2}, -\frac{1}{2} \rightarrow \frac{3}{2}, -\frac{1}{2}) \\ &- \gamma(\frac{1}{2}, -\frac{1}{2} \rightarrow \frac{3}{2}, \frac{1}{2}) \\ &- 3\gamma(\frac{1}{2}, -\frac{1}{2} \rightarrow \frac{3}{2}, \frac{3}{2})], \quad (6) \end{aligned}$$

$$\begin{aligned} \gamma_{21}^{(1)}(\frac{3}{2} \rightarrow \frac{1}{2}) &= (\sqrt{10}/3) [\gamma(\frac{3}{2}, -\frac{3}{2} \rightarrow \frac{1}{2}, -\frac{1}{2}) \\ &- \gamma(\frac{3}{2}, -\frac{3}{2} \rightarrow \frac{1}{2}, \frac{1}{2})], \quad (7) \end{aligned}$$

where the terms $\gamma(J, m \rightarrow J', m')$ represent the rates of transfer between the Zeeman substates within the 5^2P manifold. $\Gamma_1^{-1} = \tau_1$ and $\Gamma_2^{-1} = \tau_2$ are the mean lifetimes of the $5^2P_{1/2}$ and $5^2P_{3/2}$ states, respectively, which were taken as equal to one another; Svanberg¹³ found that $\tau_2 = 133 \pm 3$ ns. The multipole-decay cross sections $\sigma_{11}^{(1)}$ and $\sigma_{22}^{(L)}$ ($L=1,2,3$) are defined analogously with the gas-kinetic cross section:

$$\gamma_{11}^{(1)} = Nv\sigma_{11}^{(1)}, \quad \gamma_{22}^{(L)} = Nv\sigma_{22}^{(L)}, \quad (8)$$

where N is the buffer gas density and v is the average relative speed of the colliding atom-atom pair. The multipole relaxation cross sections $\Lambda_{11}^{(1)}$ and $\Lambda_{22}^{(L)}$ are defined as follows:¹

$$\sigma_{11}^{(1)} = \sigma_{11}^{(0)} + \Lambda_{11}^{(1)}, \quad \sigma_{22}^{(L)} = \sigma_{22}^{(0)} + \Lambda_{22}^{(L)}. \quad (9)$$

The fine-structure-mixing cross sections σ_0 are given by

$$\gamma_{ij}^{(0)}(J \rightarrow J') = Nv\sigma_0(J \rightarrow J'), \quad (10)$$

and the orientation-transfer cross sections by

$$-\gamma_{ij}^{(1)}(J \rightarrow J') = Nv\sigma_1(J \rightarrow J'), \quad (11)$$

the arrow indicating the direction of transfer. $\gamma_{11}^{(0)} = Nv\sigma_{11}^{(0)}$ and $\gamma_{22}^{(0)} = Nv\sigma_{22}^{(0)}$ are the depopulation rates for the $5^2P_{1/2}$ and $5^2P_{3/2}$ states, respectively, which are related as follows to the fine-structure-transfer rates:¹

$$\gamma_{11}^{(0)} = \sqrt{2} |\gamma_{12}^{(0)}|, \quad \gamma_{22}^{(0)} = 1/\sqrt{2} |\gamma_{21}^{(0)}|. \quad (12)$$

Equation (1) may be solved for $(n_1^{(L)}, n_2^{(L)})$:

$$\begin{pmatrix} n_1^{(L)} \\ n_2^{(L)} \end{pmatrix} = (D^{(L)})^{-1} \begin{pmatrix} \Gamma_2 + \gamma_{22}^{(L)} & -\gamma_{12}^{(L)} \\ -\gamma_{21}^{(L)} & \Gamma_1 + \gamma_{11}^{(L)} \end{pmatrix} \begin{pmatrix} s_1^{(L)} \\ s_2^{(L)} \end{pmatrix}, \quad (13)$$

where

$$D^{(L)} = (\Gamma_1 + \gamma_{11}^{(L)})(\Gamma_2 + \gamma_{22}^{(L)}) - \gamma_{12}^{(L)}\gamma_{21}^{(L)}. \quad (14)$$

Equation (13) is solved numerically with the aid of the auxiliary coefficients K_{ab}^{0L} which are directly related to the measured relative intensities of the Zeeman components in the fluorescence spectra:⁶

$$K_{ab}^{0L} = \frac{n_b^{(0)} s_a^{(L)}}{n_b^{(L)} s_a^{(0)}}, \quad a, b = 1, 2. \quad (15)$$

The two experimental modes of optical excitation correspond to the two following solutions of Eq. (13).

(i) When the $5^2P_{1/2, -1/2}$ state is optically excited, $s_2^{(L)} = 0$:

$$K_{11}^{01} = \frac{n_1^{(0)} s_1^{(1)}}{n_1^{(1)} s_1^{(0)}} = \frac{\Gamma_2 + \gamma_{22}^{(0)} D^{(1)}}{\Gamma_2 + \gamma_{22}^{(1)} D^{(0)}}, \quad (16)$$

$$K_{12}^{01} = \frac{\gamma_{21}^{(0)} D^{(1)}}{\gamma_{21}^{(1)} D^{(0)}}.$$

(ii) When the $5^2P_{3/2, -3/2}$ state is optically excited, $s_1^{(L)} = 0$:

$$K_{22}^{01} = \frac{\Gamma_1 + \gamma_{11}^{(0)} D^{(1)}}{\Gamma_1 + \gamma_{11}^{(1)} D^{(0)}}, \quad K_{22}^{02} = \frac{\Gamma_1 + \gamma_{11}^{(0)} D^{(2)}}{\Gamma_1 D^{(0)}}, \quad (17)$$

$$K_{22}^{03} = \frac{\Gamma_1 + \gamma_{11}^{(0)} D^{(3)}}{\Gamma_1 D^{(0)}}, \quad K_{21}^{01} = \frac{\gamma_{12}^{(0)} D^{(1)}}{\gamma_{12}^{(1)} D^{(0)}}.$$

$D^{(L)}$ may be obtained from Eq. (14). K_{ab}^{0L} can also be expressed in terms of the populations of the Zeeman substates, using the definitions of $n_1^{(L)}$, $n_2^{(L)}$, $s_1^{(L)}$, and $s_2^{(L)}$.^{1,5}

In the present experiment only circularly polarized radiation was detected and, consequently, the population ratios $N_{J,m}/N_{J',m'}$ are proportional to the ratios of the measured integrated intensities:

$$\frac{N_{J,m}}{N_{J',m'}} = \frac{I_{J,m}}{I_{J',m'}} \frac{A_{J',m'}^\sigma}{A_{J,m}^\sigma}, \quad (18)$$

where $A_{J,m}^\sigma$ are the appropriate Einstein A coefficients for decay of the excited states by emission of circularly polarized light,¹⁴ which are magnetic-field dependent. In weak fields they are in the ratio $A_{3/2, \pm 3/2}^\sigma : A_{3/2, \pm 1/2}^\sigma : A_{1/2, \pm 1/2}^\sigma = 3:1:2$. In strong fields, $5^2P_{1/2} - 5^2P_{3/2}$ mixing causes a change in this ratio⁴ which, in a field of 7 T, becomes $A_{3/2, \pm 3/2}^\sigma : A_{3/2, \pm 1/2}^\sigma : A_{1/2, \pm 1/2}^\sigma = 3:0.83:2.09$. The effect of the field on the A coefficients is more pronounced in the present case (fine-structure splitting equal to 18.75 cm^{-1}) than in the case of the 4^2P resonance states where the fine-structure splitting is 58 cm^{-1} .

The rates $\gamma_{12}^{(0)}$, $\gamma_{21}^{(0)}$, $\gamma_{11}^{(0)}$, and $\gamma_{22}^{(0)}$ are known from the fine-structure mixing cross sections⁶ and may be used to express $D^{(2)}$ and $D^{(3)}$ in terms of $\gamma_{22}^{(2)}$ and $\gamma_{22}^{(3)}$. Equations (16) and (17) are coupled through the product $\gamma_{12}^{(1)}\gamma_{21}^{(1)}$ contained in the expression for $D^{(1)}$. However,

we believe that $\gamma_{12}^{(1)}\gamma_{21}^{(1)}$ is small and can be neglected to a good approximation.⁶ With this simplification the multipole-relaxation cross sections $\Lambda_{11}^{(1)}$ and $\Lambda_{22}^{(L)}$ may be expressed as follows:

$$\Lambda_{11}^{(1)} = \frac{1}{N\nu\tau_1} (K_{11}^{01} - 1) + \left[\frac{K_{11}^{01}}{1 + N\nu\tau_2\sigma_{22}^{(0)}} - 1 \right] \sigma_{11}^{(0)}, \quad (19)$$

$$\Lambda_{22}^{(L)} = \frac{1}{N\nu\tau_2} (K_{22}^{0L} - 1) + \left[\frac{K_{22}^{0L}}{1 + N\nu\tau_1\sigma_{11}^{(0)}} - 1 \right] \sigma_{22}^{(0)}. \quad (20)$$

Equations (19) and (20) are used to derive the multipole relaxation cross sections from the intensities of the Zeeman fluorescent components, measured in relation to buffer gas densities. It should be noted that, if fine-structure mixing were negligible as is frequently the case when the fine-structure splitting is large, only the first terms would be significant in Eqs. (19) and (20). In the present case the second terms of Eqs. (19) and (20) contributed approximately 15% of the total cross sections.

III. EXPERIMENTAL DETAILS

A. Description of the apparatus

The arrangement of the apparatus is shown schematically in Fig. 1. Potassium atoms mixed with a noble gas and contained in a fluorescence cell placed in a 7-T magnetic field were irradiated with pulses from a N_2 laser and a pumped dye laser which excited either the $5^2P_{1/2, -1/2}$ or the $5^2P_{3/2, -3/2}$ state. The resulting circularly polarized fluorescence, monitored at right angles to the direction of excitation and parallel to the magnetic

field, consisted in each case of a direct fluorescence component emitted in the decay of the optically populated state and sensitized fluorescence components emitted from Zeeman substates populated by collisions. The left- and right-circularly polarized components were separated by a combination of a quarter-wave plate and a linear polarizer, and were further resolved with a scanning Fabry-Perot interferometer whose output was detected with a photomultiplier and accumulated in a multichannel scaler (MCS).

The N_2 laser, which was built in house, emitted light pulses of 8 ns, full width at half maximum (FWHM). These were applied transversely to a two-stage dye laser operated with a nearly saturated solution of diphenylstilbene (DPS) in *p*-dioxane contained in magnetically stirred cuvettes. The dye-laser output was condensed into an optical fiber and conveyed to the fluorescence cell. The resulting fluorescence was collected by a lens, rendered parallel, passed through the quarter-wave plate followed by a linear polarizer, and made incident onto the mirrors of a piezoelectrically scanned Fabry-Perot interferometer. The interferometer output was collimated and focused on the photocathode of an ITT FW130 refrigerated photomultiplier whose output pulses were amplified by an Ortec 9302 amplifier discriminator, sent to a gated inverter amplifier, and collected in a 1024-channel MCS. The accumulated spectrum was transferred for further analysis to a Commodore PET 2001 computer which also produced plots of the integrated intensities of the fluorescence components. The areas of the fluorescence peaks were individually calculated after correction for background noise.

The quartz fluorescence cell had a square cross section ($2.5 \times 2.5 \times 4.0$ cm³) and was fitted with a 1-cm-long sidearm which contained a small quantity of metallic potassium and protruded downwards. The body of the cell was enclosed in an oven heated by oil circulating from a Neslab ultrathermostat. The sidearm was heated separately, and its temperature controlled the potassium vapor pressure in the cell. The temperatures were measured with several copper-constantan thermocouples located at various points on the cell and sidearm. The oven and cell were located in the center of the bore of a superconducting solenoid (Oxford Instruments, Model S7/123/1) which was capable of generating magnetic fields up to 7 T with 0.1% homogeneity. The cell was connected by a narrow-bore tube and a greaseless stopcock to a vacuum and gas-filling system from which buffer gasses were admitted as required. The gases (research grade) were supplied by the Matheson Company. Gas pressures which ranged from 20 to 160 mTorr were measured with an MKS Baratron capacitance gauge.

The piezoelectrically scanned interferometer (Burleigh, model 110) was fitted with $\lambda/200$ aluminized mirrors and had a finesse of 30. In order to ensure the proper stability of the interferometer, as well as the scan-to-scan reproducibility required for signal averaging, its alignment was locked to the interference pattern of the He-Ne laser line, which was scanned during the initial 0.15 s of each interferometer sweep and provided the reference

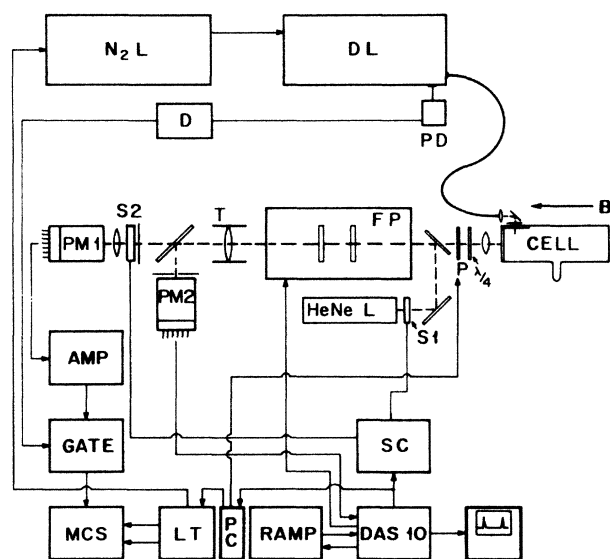


FIG. 1. Schematic arrangement of the apparatus. N_2L , nitrogen laser; DL , dye laser; PD , photodiode; D , delay line; FP , Fabry-Perot interferometer; T , telescope; $PM1, PM2$, photomultipliers; $S1, S2$, shutters; AMP , amplifier discriminator; $GATE$, gated pulse-inverter amplifier; LT , channel advance laser trigger; SC , shutter controller; PC , polarizer controller. B indicates the 7-T field.

for the Burleigh DAS10 stabilizer controlling the piezoelectric elements. A parallel beam of He-Ne laser light was made incident on the mirrors of the interferometer by a plane-glass beam splitter located between the interferometer and the linear polarizer. After transmission through the interferometer, a part of the light beam was conveyed by a second beam splitter to a second photomultiplier PM2 whose amplified signal was applied to the DAS10 unit to stabilize and align the mirrors of the interferometer. The He-Ne laser light was prevented from interfering with the fluorescence detection system by two shutters, S1 positioned in front of the laser and S2 in front of the photomultiplier PM1. The operating cycle of S1 and S2 was controlled by an electronic timer and was locked to the interferometer sweep by the trigger output of the ramp generator.

The interferometer, which had a free spectral range of 12.5 cm^{-1} , was scanned through approximately 2.5 interference orders. Each scan required 2 s and during each scan the photomultiplier output pulses resulting from laser excitation were sent to the MCS whose start was triggered by the start of the interferometer scan, and the channel advance rate was synchronized with the triggering of the laser. Because of the limitations of the DAS10 stabilizer which restricted the maximal scanning time to 2 s, and of the N_2 laser which was stable at repetition rates not exceeding 40 Hz, it was not possible to register fluorescence signals consecutively in all 256 channels during a single scan, and four scans were needed to cover the 256 channels. This was accomplished by having the MCS channel advance triggered at four times the laser repetition rate and, with this repetition rate set at 34.5 Hz, the fluorescence spectrum was accommodated within the 256 memory channels. The addition of the polarization analyzer to improve the spectral resolution required the use of two 256-channel segments of the MCS memory, one to register the σ^+ components and the other to register the σ^- components of the spectrum. This was accomplished by having two linear polarizers (Polaroid HN38) oriented with their optical axes at 90° to each other, mounted on a rotating platform. The rotation of the platform (and orientation of the polarizer) was controlled by a stepper motor synchronized to the interferometer. A small number of channels was not used for fluorescence detection as the DAS10 stabilizer system required 0.15 s operation time per interferometer sweep and the polarizer rotator required about 80 ms to complete its rotation.

In order to avoid the registration of signals due to scattered dye-laser light, the pulse inverter amplifier was gated. The gate was triggered by the signal of a photodiode which monitored the dye-laser output pulses. The variable data-acceptance window of the inverter amplifier extended from 30 ns after the start of the laser pulse to 1400 ns ($\sim 10\tau$). Another effect of the gating was to increase artificially the measured ratios of sensitized-to-direct fluorescence, since the direct component is derived from the primarily laser-excited state while the sensitized components arise from states which become gradually populated by collisional transfer. To correct the intensity ratios for the 30-ns time delay, we

used a computer simulation of Eq. (2) in which the laser pulse was simulated by

$$s(t) = \begin{cases} A \sin(\pi t / 10) & (0 \leq t \leq 10 \text{ ns}) \\ 0 & (t > 10 \text{ ns}), \end{cases} \quad (21)$$

where $t/10$ is a ratio of times in nanoseconds. The components γ_{ij} were taken from the experimental data as a first approximation and the intensity or population ratios obtained from the simulation for time delays of 0 and 30 ns were compared in an iterative procedure. It was found that the measured integrated-intensity ratios indeed required corrections for the time delay. When using the $5^2P_{3/2,-3/2}$ excitation mode, the resulting intensity ratios required a correction factor 0.74; with $5^2P_{1/2,-1/2}$ excitation, the intensity ratios required a correction factor 0.75.

B. Experimental procedure

Before each experimental run, the fluorescence cell was pumped down to 5×10^{-6} Torr and isolated from the vacuum system. For about 12 h, the main oven was kept at 115°C and the sidearm at 15°C to ensure the condensation of all the potassium in the sidearm. The cell was again opened to the vacuum system and maintained for 1–2 h at 5×10^{-6} Torr with the sidearm at 95°C . Finally, the cell was flushed with clean buffer gas, pumped down, and filled with an appropriate quantity of gas to begin the experiment. After a short time, during which the gas pressure in the cell reached equilibrium, the cell stopcock was closed. The sidearm temperature was held at 95°C in order to obtain a satisfactory signal-to-noise ratio. At this temperature the vapor pressure is 1.2×10^{-5} Torr and radiation trapping has a negligible effect on the lifetime of the 5^2P state.

The coarse tuning of the dye laser to excite the $5^2P_{1/2}$ or $5^2P_{3/2}$ fine-structure substate in zero field was accomplished by observing the fluorescence produced in a warm Osram lamp. The fine tuning to excite a specific Zeeman sublevel was effected by maximizing the fluorescence signal while adjusting the voltage in a piezoelectric transducer which acted as the stop for the tuning-grating arm in the dye-laser oscillator cavity. Thus it was possible to excite selectively each Zeeman sublevel, including the π transitions which were not observed in fluorescence.

The fluorescence count rate was adjusted to produce 2–4 counts per MCS sweep (140 laser pulses), by varying the output power of the N_2 laser and the degree of focusing of the dye-laser beam into the optical fiber which conveyed it to the fluorescence cell. A termination of the optical fiber conducting exciting radiation from the dye laser, which was attached to the side window, produced a parallel beam of light in the cell, 2 mm in diameter and passing 2 mm from the observation window. The tuning of the dye laser was alternated between $5^2P_{1/2,-1/2}$ and $5^2P_{3/2,-3/2}$ modes of excitation. An average of 8 h of continuous running was required in order to record the fluorescence spectrum resulting from either mode of excitation. In each case the observed

spectrum consisted of circularly polarized σ^+ and σ^- components emitted in the decays of the 5^2P Zeeman states as shown in Fig. 2. After a scan of the fluorescence spectrum using one mode of excitation, the cell was pumped down to 5×10^{-6} Torr, refilled with new gas at the same pressure, and the scan was begun using the second mode of excitation. The gas was changed after each run to avoid contamination, the absence of which was tested by comparing the results of the experiment against a fluorescence spectrum obtained when the cell was isolated from the vacuum system. It was found that there was no noticeable difference between the spectra when the cell was sealed for less than 18 h. After longer periods of time, differences in the spectra became apparent and consequently the gas was changed every 8–10 h to ensure its purity. This was particularly important at the lower gas pressures.

IV. RESULTS AND DISCUSSION

A trace of the fluorescence spectrum obtained with $5^2P_{1/2, -1/2}$ excitation in the presence of 50 mTorr Ar is shown in Fig. 3. The fluorescence peaks are identified as arising from the transitions labeled A–F in Fig. 2. The σ^+ and σ^- components of the spectrum were detected and registered separately as described in Sec. III B and are thus presented in Fig. 3, in which all six fluorescence peaks are clearly resolved. The two polarization components of the spectrum contain small contributions of opposite polarization which arise from a slight “leakage” through the linear polarizer, amounting to less than 5% of the total fluorescent intensity, which introduced a negligibly small error into the measured cross sections. The trace represents typical data accumulated during an 8-h run and consisting of over 30 000 counts. A similar trace of the fluorescence spectrum produced with $5^2P_{3/2, -3/2}$ excitation in the presence of 150 mTorr Ne

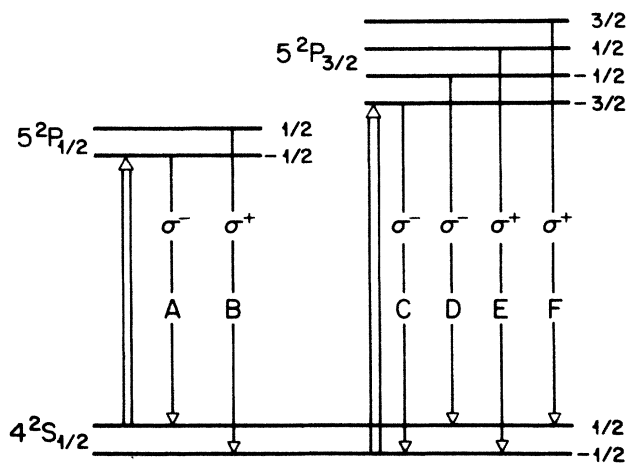


FIG. 2. Energy-level diagram of the 5^2P Zeeman substates in potassium, showing their σ decays to the ground state. Either the $5^2P_{1/2, -1/2}$ or the $5^2P_{3/2, -3/2}$ substate is optically excited; all other substates are populated by collisions. The π transitions are not shown; the spacings between the levels are not drawn to scale.

is shown in Fig. 4. There it may be seen that the sensitized fluorescence peaks are relatively more intense in comparison with the direct fluorescence peak C, than in Fig. 3 which corresponds to a significantly lower buffer-gas pressure. The resolution of the Zeeman components is considerably better than might be apparent from Figs. 3 and 4 in which the scale of the interferograms has been compressed. The integrated intensities of all the components in the fluorescence spectra were corrected for the time delay as described in Sec. III A, and the ratios of sensitized-to-direct fluorescence intensities are plotted in relation to the buffer-gas pressures in Figs. 5 and 6 for Ar, Figs. 7 and 8 for Ne, and Figs. 9 and 10 for He. As may be seen in Figs. 5–10, the integrated intensity ratios have been multiplied by the appropriate $A_{j,m}^{\sigma}$ coefficients to yield plots which actually represent the population ratios of collisionally-to-directly (optically) populated Zeeman sublevels in the 5^2P Zeeman manifold. As expected, the plots are linear over a range of buffer-gas pressures extending from 20 mTorr (He) to 160 mTorr (Ar). The linearity of the plots suggests the absence of multiple collisional transfers, including back transfer. These data, in conjunction with Eqs. (19) and (20), yielded the multipole-relaxation cross sections $\Lambda^{(L)}$ which are listed in Table I. The individual Zeeman mixing cross sections $Q(J, m - J', m')$ have also been calcu-

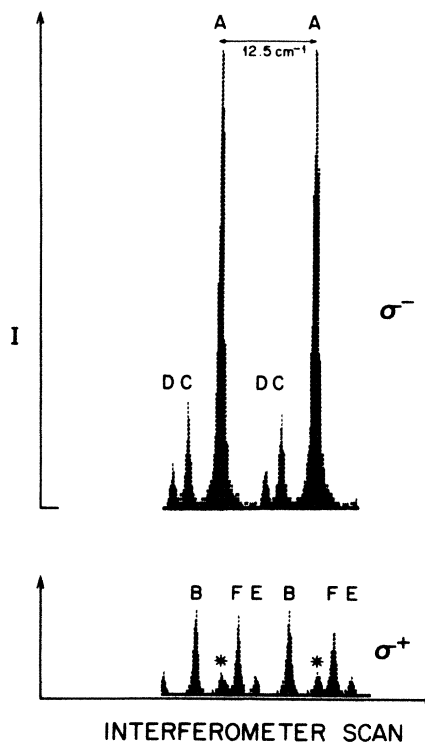


FIG. 3. A trace of the Zeeman fluorescence spectrum emitted from potassium vapor mixed with 50 mTorr Ar. The $5^2P_{1/2, -1/2}$ state is optically excited and the peaks are labeled to correspond to the transitions indicated in Fig. 2. The free spectral range of the interferometer is 12.5 cm^{-1} . The asterisks (*) indicate components due to polarizer leakage.

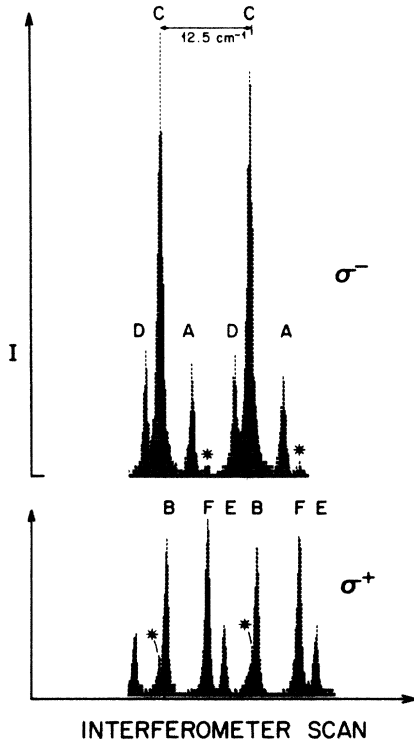


FIG. 4. A trace of the Zeeman fluorescence spectrum emitted from potassium vapor mixed with 150 mTorr Ne. The $5^2P_{3/2, -3/2}$ state is optically excited and the peaks are labeled to correspond to the transitions indicated in Fig. 2. The free spectral range of the interferometer is 12.5 cm^{-1} . The asterisks (*) indicate components due to polarizer leakage.

lated from these data and are presented in Table II. The data in Table II show a trend which has been noted in some previous experiments, namely, that Ne cross sections are relatively small, compared with He and Ar values.^{2,15} The last entry in the table is the cross section $Q(\frac{3}{2}, -\frac{1}{2} \rightarrow \frac{3}{2}, \frac{1}{2})$ which was not determined experimentally but may be calculated from the other cross sections using the following relation, which results from the fact that the hexadecapole-relaxation rate $\gamma^{(4)}$ equals zero:^{16,17}

$$\begin{aligned}
 & Q\left(\frac{3}{2}, -\frac{1}{2} \rightarrow \frac{3}{2}, \frac{1}{2}\right) \\
 &= \frac{4}{3}Q\left(\frac{3}{2}, -\frac{3}{2} \rightarrow \frac{3}{2}, -\frac{1}{2}\right) - \frac{4}{3}Q\left(\frac{3}{2}, -\frac{3}{2} \rightarrow \frac{3}{2}, \frac{1}{2}\right) \\
 &+ Q\left(\frac{3}{2}, -\frac{3}{2} \rightarrow \frac{3}{2}, \frac{3}{2}\right). \quad (22)
 \end{aligned}$$

The analysis of the fluorescent Zeeman spectrum also yielded the cross sections σ_1 for the transfer of orientation and σ_0 for fine-structure mixing as shown in Table III. The latter cross sections provide a useful check of these determinations against the results of the experiments carried out in zero magnetic field.¹⁸ This comparison is made in Table III in which the zero-field cross sections Q (Ref. 18) have been multiplied by normalizing factors reflecting the statistical weights of the excited states. Thus, in accordance with Eqs. (4) and (5),

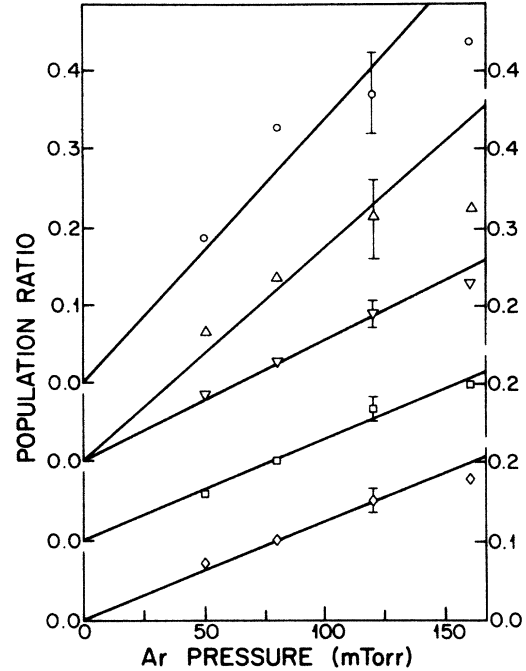


FIG. 5. Plots of Zeeman fluorescent intensity (and population) ratios arising from $5^2P_{3/2, -3/2}$ excitation, showing effects of Zeeman mixing induced in K-Ar collisions. The separate origin for each plot is indicated on the vertical axis. The error bars represent statistical scatter of the measurements. Each point represents the intensity ratio of the specified components, multiplied by the ratio of the appropriate $A_{J,m}^g$ coefficients. \diamond , $3I(A)/2.09I(C)$; \square , $I(F)/I(C)$; ∇ , $3I(E)/0.83I(C)$; \circ , $3I(D)/0.83I(C)$; \triangle , $3I(B)/2.09I(C)$.

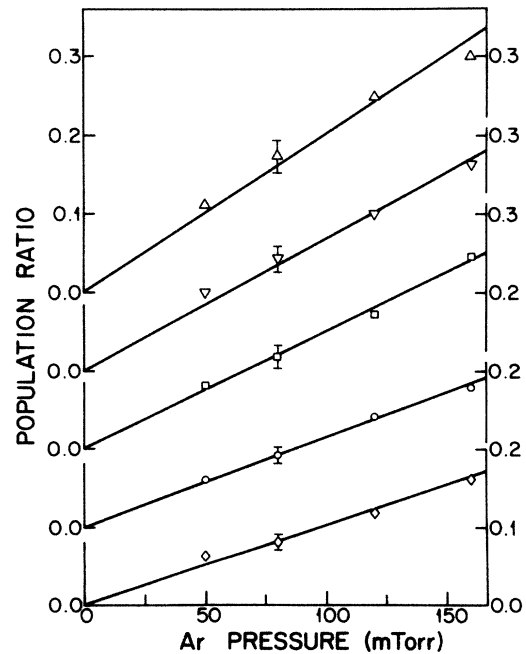


FIG. 6. Plots of Zeeman fluorescent intensity ratios arising from $5^2P_{1/2, -1/2}$ excitation, against Ar pressure. For a description see Fig. 5. \diamond , $2.09I(E)/0.83I(A)$; \circ , $2.09I(F)/3I(A)$; \square , $2.09I(C)/3I(A)$; ∇ , $I(B)/I(A)$; \triangle , $2.09I(D)/0.83I(A)$.

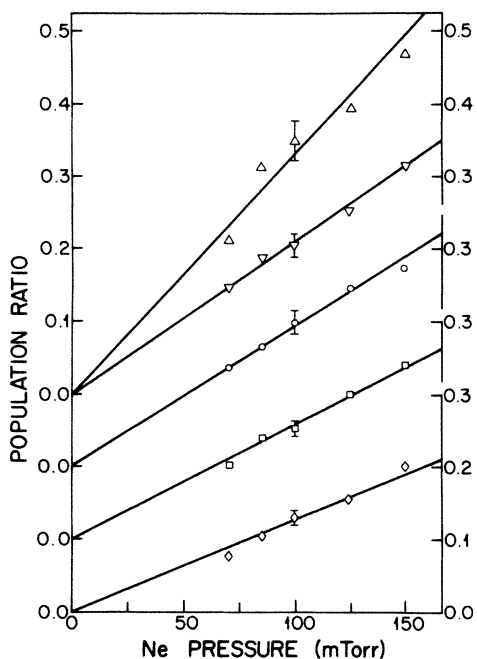


FIG. 7. Plots of Zeeman fluorescent intensity ratios arising from $5^2P_{3/2, -3/2}$ excitation, against Ne pressure. For a description see Fig. 5. \diamond , $3I(A)/2.09I(C)$; \square , $I(F)/I(C)$; \circ , $3I(B)/2.09I(C)$; ∇ , $3I(E)/0.83I(C)$; \triangle , $3I(D)/0.83I(C)$.

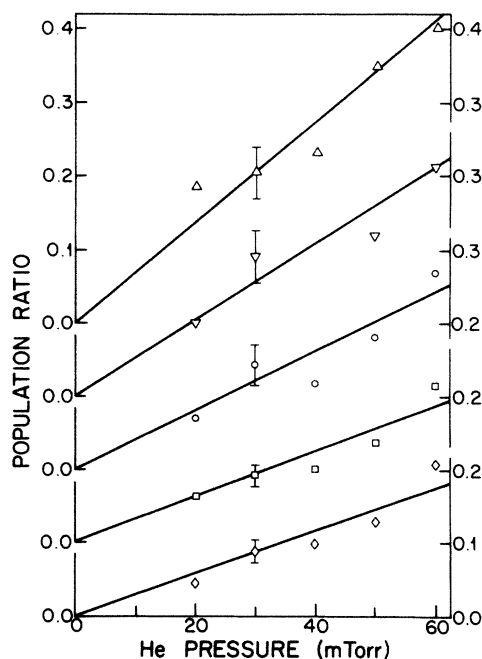


FIG. 8. Plots of Zeeman fluorescent intensity ratios arising from $5^2P_{1/2, -1/2}$ excitation, against He pressure. For a description see Fig. 5. \diamond , $2.09I(F)/3I(A)$; \square , $2.09I(E)/0.83I(A)$; \circ , $2.09I(C)/3I(A)$; ∇ , $I(B)/I(A)$; \triangle , $2.09I(D)/0.83I(A)$.

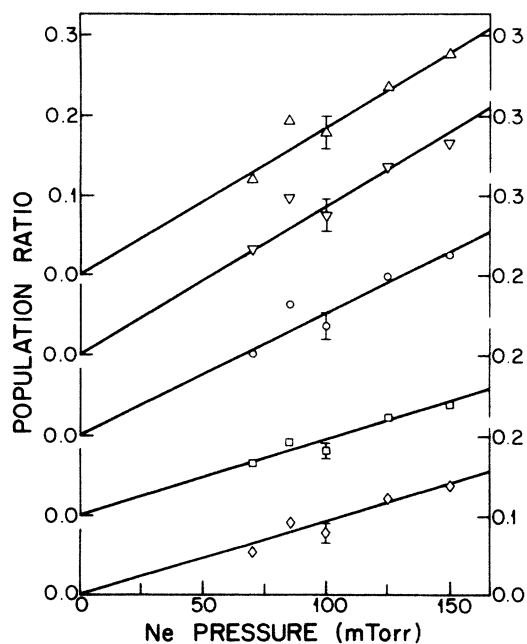


FIG. 9. Plots of Zeeman fluorescent intensity ratios arising from $5^2P_{3/2, -3/2}$ excitation, against He pressure. For a description see Fig. 5. \diamond , $I(F)/I(C)$; \square , $3I(A)/2.09I(C)$; \circ , $3I(E)/0.83I(C)$; ∇ , $3I(B)/2.09I(C)$; \triangle , $3I(D)/0.83I(C)$.

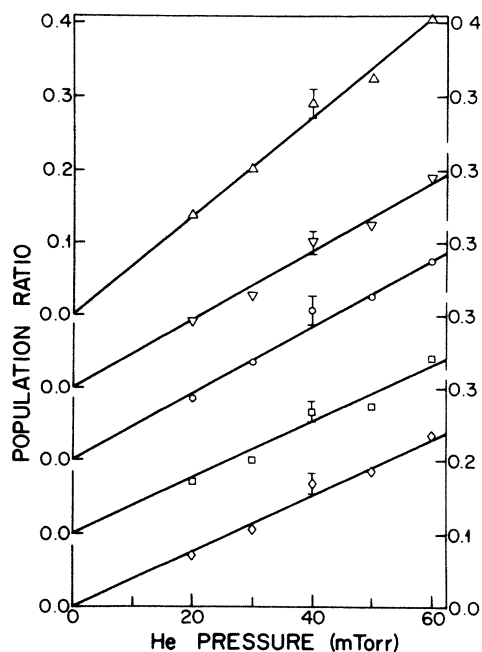


FIG. 10. Plots of Zeeman fluorescent intensity ratios arising from $5^2P_{1/2, -1/2}$ excitation, against He pressure. For a description see Fig. 5. \diamond , $2.09I(F)/3I(A)$; \square , $2.09I(E)/0.83I(A)$; \circ , $2.09I(C)/3I(A)$; ∇ , $I(B)/I(A)$; \triangle , $2.09I(D)/0.83I(A)$.

TABLE I. 5^2P multipole-relaxation cross sections (\AA^2).

Designation	Collision partner		
	He	Ne	Ar
$\Lambda_{11}^{(1)}$	170 ± 37^a	201 ± 30^a	204 ± 16^a
	40.6^b	258^b	109^b
$\Lambda_{22}^{(1)}$	326 ± 86^a	421 ± 41^a	399 ± 27^a
	155^b	340^b	253^b
$\Lambda_{22}^{(2)}$	811 ± 247^a	873 ± 187^a	884 ± 110^a
	256^b	725^b	504^b
$\Lambda_{22}^{(3)}$	1414 ± 576^a	1388 ± 475^a	2672 ± 1117^a
	236^b		438^b

^aThis experiment.^bReference 9.

$$\sigma_0(\frac{1}{2} \rightarrow \frac{3}{2}) = (1/\sqrt{2})Q_{12}, \quad \sigma_0(\frac{3}{2} \rightarrow \frac{1}{2}) = \sqrt{2}Q_{21}. \quad (23)$$

It may be seen in Table III that there is satisfactory agreement between the two sets of experimentally determined cross sections for Ne and Ar; for He the agreement is not nearly as good. Equations (6) and (7) show that the cross sections σ_1 (which are quite small) are obtained from the sums and differences of much larger cross sections and this renders them subject to considerable error. A comparison with the K 4^2P and Na 3^2P multipole-relaxation and Zeeman mixing cross sections might also be of some interest. The cross sections listed in Tables I–III are significantly larger than those determined for the 4^2P K atoms^{4,5} and are somewhat larger than the cross sections for the Na 3^2P resonance states² whose fine-structure splitting is similar to that of the K 5^2P states.

The multipole-relaxation cross sections and transfer cross sections listed in Tables I and III may also be compared with the calculations of Spielfiedel *et al.*⁹ It may be seen in Table I that there is agreement within an order of magnitude between our relaxation cross sections and those calculated by Spielfiedel *et al.* Although these

TABLE II. Zeeman-mixing cross sections $Q(J, m - J', m')$ (\AA^2).

Designation	Collision partner		
	He	Ne	Ar
$Q(\frac{1}{2}, -\frac{1}{2} \rightarrow \frac{1}{2}, \frac{1}{2})$	93 ± 7	75 ± 9	86 ± 11
$Q(\frac{1}{2}, -\frac{1}{2} \rightarrow \frac{3}{2}, \frac{3}{2})$	76 ± 6	35 ± 5	55 ± 2
$Q(\frac{1}{2}, -\frac{1}{2} \rightarrow \frac{3}{2}, \frac{1}{2})$	75 ± 7	36 ± 4	50 ± 6
$Q(\frac{1}{2}, -\frac{1}{2} \rightarrow \frac{3}{2}, -\frac{1}{2})$	139 ± 4	74 ± 8	99 ± 8
$Q(\frac{1}{2}, -\frac{1}{2} \rightarrow \frac{3}{2}, -\frac{3}{2})$	93 ± 7	62 ± 3	70 ± 5
$Q(\frac{3}{2}, -\frac{3}{2} \rightarrow \frac{3}{2}, \frac{3}{2})$	55 ± 10	61 ± 3	61 ± 5
$Q(\frac{3}{2}, -\frac{3}{2} \rightarrow \frac{3}{2}, \frac{1}{2})$	78 ± 15	81 ± 3	74 ± 5
$Q(\frac{3}{2}, -\frac{3}{2} \rightarrow \frac{3}{2}, -\frac{1}{2})$	144 ± 26	127 ± 11	159 ± 29
$Q(\frac{3}{2}, -\frac{3}{2} \rightarrow \frac{1}{2}, \frac{1}{2})$	106 ± 17	75 ± 3	127 ± 26
$Q(\frac{3}{2}, -\frac{3}{2} \rightarrow \frac{1}{2}, -\frac{1}{2})$	61 ± 9	49 ± 4	61 ± 7
$Q(\frac{3}{2}, -\frac{1}{2} \rightarrow \frac{3}{2}, \frac{1}{2})$	143 ± 34	121 ± 15	175 ± 35

TABLE III. Fine-structure-mixing and orientation-transfer cross sections (\AA^2).

Designation	Collision partner		
	He	Ne	Ar
$\sigma_0(\frac{1}{2} \rightarrow \frac{3}{2})$	271 ± 45^a	146 ± 14^a	194 ± 24^a
	397 ± 59^b	139 ± 20^b	224 ± 32^b
	156^c	77^c	139^c
$\sigma_0(\frac{3}{2} \rightarrow \frac{1}{2})$	236 ± 35^a	175 ± 18^a	266 ± 33^a
	376 ± 55^b	139 ± 25^b	216 ± 31^b
$\sigma_1(\frac{1}{2} \rightarrow \frac{3}{2})$	-36 ± 14^a	-37 ± 15^a	-30 ± 12^a
	-66^c	-22^c	-52^c
$\sigma_1(\frac{3}{2} \rightarrow \frac{1}{2})$	$+47 \pm 35^a$	$+28 \pm 11^a$	$+70 \pm 28^a$

^aThis experiment.^bReference 18.^cReference 9.

authors appear to define the multipole-relaxation cross sections as described in Sec. II above, it is not clear how their orientation-transfer cross sections σ_1 and fine-structure-mixing cross sections σ_0 are defined and this makes the comparison attempted in Table III rather uncertain.

The calculations of Spielfiedel *et al.*⁹ were based on the interatomic model potentials of Pascale and Vandepanque,¹⁹ and were carried out semiclassically (using a straight-line trajectory approximation) as well as quantum mechanically. In all the calculations the authors employed the impact approximation and neglected coupling to states other than 5^2P ; their principal aim was the treatment of pressure broadening and shift of the spectral lines arising from the 5^2P - 4^2S decays. It is not surprising that the agreement with our cross sections is not particularly good; the best agreement is shown in the case of Ne, though the authors express some considerable doubt as to the potential which they employed.⁹ Since the results of these calculations depend strongly on the model potentials used, a recalculation of the cross sections using more accurate alkali-metal–noble-gas potentials²⁰ would provide a more valid comparison between theory and experiment.

The limits of error attributed to the various cross sections listed in Tables I–III arise from both statistical and systematic sources. The statistical error is inherent in the photon counting procedure used to obtain the fluorescence intensities and also includes a contribution due to variations in the pulse amplitudes of the pumping laser. The laser power was adjusted to maintain a steady count rate and the pulse-to-pulse variation was averaged over the 8-h recording time. Error due to “pile up” was most probably eliminated by maintaining a low count rate of 2–4 pulses per interferometer scan, which was established experimentally; it was found that pile up became negligible at counting rates less than 6 pulses per scan. There are also several sources of systematic error. The time delay between the excitation and detection of the fluorescence is of significance and the effect produced

by it was corrected by an iterative process of computer modeling of the radiative decays. We believe this to be the first direct experimental determination of all the multipole-relaxation cross sections for a state lying above the resonance state in an alkali-metal atom, induced by collisions with noble-gas atoms.

ACKNOWLEDGMENTS

The authors wish to express their appreciation to Dr. W. E. Baylis for helpful discussions. This research was supported by a grant from the Natural Sciences and Engineering Research Council of Canada.

-
- ¹W. E. Baylis, in *Progress in Atomic Spectroscopy, Part B*, edited by W. Hanle and H. Kleinpoppen (Plenum, New York, 1979).
- ²J.-C. Gay and W. B. Schneider, *Z. Phys. A* **278**, 211 (1976).
- ³J.-C. Gay and W. B. Schneider, *Phys. Rev. A* **20**, 905 (1979).
- ⁴R. Boggy and F. A. Franz, *Phys. Rev. A* **25**, 1887 (1982).
- ⁵P. Skalinski and L. Krause, *Phys. Rev. A* **26**, 3338 (1982).
- ⁶R. W. Berends, P. Skalinski, and L. Krause, *J. Phys. B* **17**, 605 (1984).
- ⁷E. L. Lewis, C. S. Wheeler, and A. D. Wilson, *J. Phys. B* **10**, 2619 (1977).
- ⁸C. G. Carrington, D. N. Stacey, and J. Cooper, *J. Phys. B* **6**, 417 (1973).
- ⁹A. Spielfiedel, D. Gilbert, E. Roueff, and F. Rostas, *J. Phys. B* **12**, 3693 (1979).
- ¹⁰R. B. Bulos and W. Happer, *Phys. Rev. A* **4**, 849 (1971).
- ¹¹P. Pace and J. B. Atkinson, *Can. J. Phys.* **52**, 1635 (1974).
- ¹²M. Elbel, in *Progress in Atomic Spectroscopy, Part B*, edited by W. Hanle and H. Kleinpoppen (Plenum, New York, 1979).
- ¹³S. Svanberg, *Phys. Scripta* **4**, 275 (1971).
- ¹⁴A. C. G. Mitchell and M. W. Zemansky, *Resonance Radiation and Excited Atoms* (Cambridge University Press, Cambridge, England, 1934).
- ¹⁵W. Berdowski and L. Krause, *Phys. Rev.* **165**, 158 (1968).
- ¹⁶M. I. Dyakonov and V. I. Perel, *Zh. Eksp. Teor. Fiz.* **48**, 345 (1965) [*Sov. Phys.—JETP* **21**, 227 (1965)].
- ¹⁷W. E. Baylis (private communication).
- ¹⁸R. W. Berends, W. Kedzierski, and L. Krause, *J. Quant. Spectrosc. Radiat. Transfer* **37**, 157 (1987).
- ¹⁹J. Pascale and J. Vandeplanque, *J. Chem. Phys.* **60**, 2278 (1974).
- ²⁰See, for example, J. Pascale, *Phys. Rev. A* **28**, 632 (1983); F. Rebrost, R. Best, and W. Behmenburg, *J. Phys. B* **20**, 2627 (1987).